J-Coupling Restraints in RNA Structure Determination

JOHN P. MARINO,*,† HARALD SCHWALBE,‡ AND CHRISTIAN GRIESINGER‡

Center for Advanced Research in Biotechnology, 9600 Gudelsky Drive, Rockville, Maryland 20850, and Institut für Organische Chemie, Universität Frankfurt, Marie-Curie Strasse 11, Frankfurt/Main D-60439, Germany

Received July 22, 1998

Introduction

In nuclear magnetic resonance (NMR) structural studies of macromolecules in solution, magnetic interactions between nuclei, known variously as spin−spin couplings, scalar couplings, or *J*-couplings, can provide information about molecular bond geometry. Among measured *J*-couplings, vicinal ^3J-couplings, which involve nuclei separated by three bonds, are generally the most structurally informative. Vicinal couplings can be correlated, using theoretical relations derived by Karplus,[1] to the dihedral angle between the terminal bonds. In RNA oligonucleotides, vicinal ^3J(H,H), ^3J(H,C), ^3J(H,P), and ^3J(C,P) couplings can be used to define the dihedral angles which determine sugar pucker, glycosidic bond angle, and phosphodiester backbone angles (Figure 1). Additionally, ^1J(H,C) and ^2J(H,C) couplings can be qualitatively related to sugar pucker and can provide in certain instances stereospecific assignment of geminal proton resonances. Here we present an overview of recent NMR methods developed to measure *J*-couplings in ^{13}C,^{15}N-labeled RNA. The importance of dihedral restraints in RNA structure determination is also discussed.

Background

As shown in Figure 1, the nucleotide phosphodiester backbone in RNA is defined by a total of six backbone torsion angles (α, β, γ, δ, ϵ, ζ). The glycosidic bond that links the ribose and base is defined by the torsion angle χ, and the ribose sugar geometry is defined by the five endocyclic torsion angles (ν_0 through ν_4). For steric reasons, the phosphodiester backbone torsion angles are normally found in one of the three staggered conformations (gauche$^+$, gauche$^-$, or trans) and the glycosidic bond angle χ is found in either the syn (0−90°) or anti (180−270°) conformation relative to the ribose. Since the ribose is a closed ring, the magnitudes of the five endocyclic torsion angles are all interrelated. The ribose geometry can therefore be defined in good approximation by two parameters, the pseudorotation phase angle, *P*, and the pucker amplitude, ν_{max}.[2] For energetic reasons, the ribose ring is never planar, but rather puckers in either an envelope (E) or twist (T) form. In the pseudorotation cycle, the ribose pucker is most often found in either the C2′-endo (South, $P = 137-194°$) or C3′-endo (North, $P = -1-34°$) region, which are its lowest energy states.[3] RNA backbone torsion angle definitions and values for the two common helical geometries, A-form and B-form, found in RNA are given in Table 1.

The sugar pucker and backbone torsion angle, δ (C5′−C4′−C3′−O3′), can be determined by measuring a series of ^3J(H,H) and ^3J(H,C) scalar couplings (Table 2). ^3J(H1′,H2′) and ^3J(H3′,H4′) couplings are both sensitive to whether the ribose sugar is in one of the two preferred conformational states, C3′-endo or C2′-endo (Figure 2). For the C2′-endo sugar pucker, the ^3J(H1′,H2′) coupling is expected to be relatively large (8−10 Hz) while the ^3J(H3′,H4′) coupling is expected to be small (<2 Hz). The opposite behavior is observed for these couplings in a C3′-endo sugar pucker. In contrast, the magnitude of the ^3J(H2′,H3′) coupling constant is about the same in these two states. Intermediate couplings are normally interpreted to indicate conformational heterogeneity between two or more sugar pucker states in fast exchange, and the relative equilibrium populations are then estimated from the size of the couplings. However, the unambiguous determination of the conformational equilibrium between two conformers requires the determination of five parameters: the pseudorotation phases P^{I} and P^{II}, the amplitudes ν_{max}^{I} and ν_{max}^{II}, and the relative populations. Thus, the possibility of an unusual sugar conformation cannot be excluded with only three ^3J(H,H) couplings. The distinction between a multistate equilibrium and a unique conformation can be made in principle by measuring additional ^3J(H,C) couplings.[4,5] ^2J(C1′,H2′), ^2J(C2′,H3′), ^2J(C3′,H2′), and ^2J(C4′,H3′) couplings (Figure 2) can also

John P. Marino was born in New York City, NY, in 1967. He graduated from Princeton University in chemistry in 1989 and completed a Ph.D. in chemistry from Yale University under the supervision of Professor Donald M. Crothers in 1995. He was an Alexander von Humboldt postdoctoral fellow with Professor Christian Griesinger at the J. W.-Goethe Universität in Frankfurt, Germany, from 1995 through 1997. He is currently a research chemist at NIST and Adjunct Assistant Professor at the Center for Advanced Research in Biotechnology in Rockville, MD.

Harald Schwalbe was born in Frankfurt, Germany, in 1966. He graduated from the J. W.-Goethe Universität in Frankfurt in chemistry in 1991 and completed his Ph.D. in organic chemistry in Frankfurt under the supervision of Professor Christian Griesinger in 1993. He was an EU supported postdoctoral fellow with Professor Christopher Dobson at Oxford University, U.K., from 1993 through 1995. He is currently a Habilitant at the Institut für Organische Chemie at the J. W.-Goethe Universität in Frankfurt, Germany.

Christian Griesinger was born in Ulm, Germany, in 1960. He graduated from the J. W.-Goethe Universität in Frankfurt, Germany, in chemistry in 1984 and completed his Ph.D. in organic chemistry in Frankfurt under the supervision of Professor Horst Kessler in 1986. He was a postdoctoral fellow with Professor R. R. Ernst at the ETH in Zürich, Switzerland, from 1986 through 1990. He is currently Professor of Chemistry in the Institut für Organische Chemie at the J. W.-Goethe Universität in Frankfurt, Germany.

† Center for Advanced Research in Biotechnology.
‡ Universität Frankfurt.

10.1021/ar9600392 CCC: $18.00
Published on Web 03/31/1999

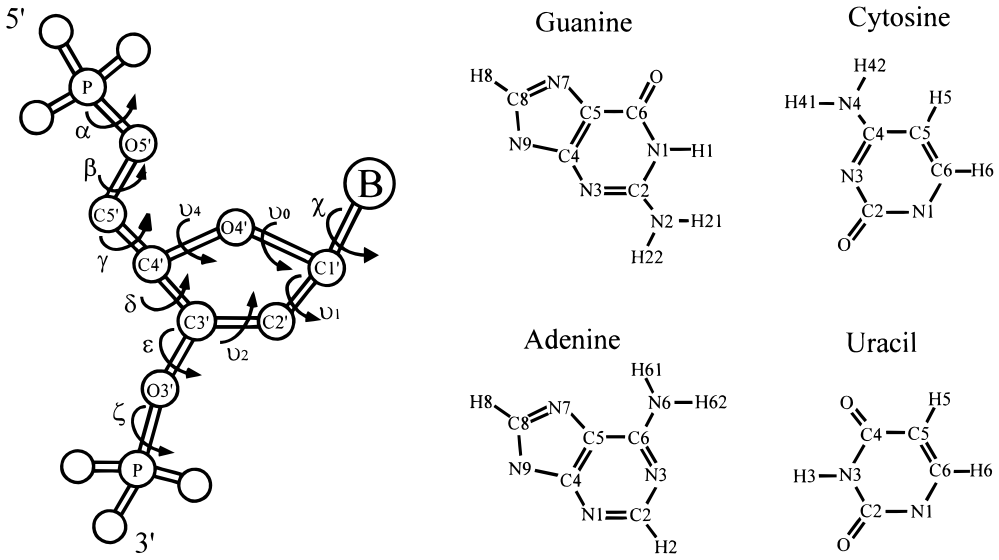

FIGURE 1. Schematic of the torsion angles (α, β, γ, δ, ϵ, ζ, ν_{0-4}, and χ) that define the nucleotide backbone geometry in RNA, where B is one of the four different aromatic bases, guanine, adenine, cytosine, and uracil, that are shown. (Adapted from ref 3, p 14).

Table 1. Definition of the Ribose and Phosphodiester Backbone Dihedral Angles of a Nucleotide Subunit in RNA and the Idealized Torsion Angles Found in A-Form and B-Form Helical Geometries[3]

angle	definition	A-form value (deg)		B-form value (deg)	
α	$O3'_{i-1}-P_i-O5'_i-C5'_i$	292	gauche$^-$	314	gauche$^-$
β	$P_i-O5'_i-C5'_i-C4'_i$	178	trans	213	trans
γ	$O5'_i-C5'_i-C4'_i-C3'_i$	54	gauche$^+$	36	gauche$^+$
δ	$C5'_i-C4'_i-C3'_i-O3'_i$	82	gauche$^+$	157	gauche$^+$
ϵ	$C4'_i-C3'_i-O3'_i-P_{i+1}$	207	trans	155	trans
ζ	$C3'_i-O3'_i-P_{i+1}-O5'_{i+1}$	289	gauche$^-$	264	gauche$^-$
ν_0	C4′−O4′−C1′−C2′	5.8	C3′-endo	−4.2	C2′-endo
ν_1	O4′−C1′−C2′−C3′	−26.2	C3′-endo	24.9	C2′-endo
ν_2	C1′−C2′−C3′−C4′	36.5	C3′-endo	−34.9	C2′-endo
ν_3	C2′−C3′−C4′−O4′	−33.0	C3′-endo	33.3	C2′-endo
ν_4	C3′−C4′−O4′−C1′	16.8	C3′-endo	−18.3	C2′-endo
χ (pyrimidine)	O4′−C1′−N1−C2	202	anti	262	anti
χ (purine)	O4′−C1′−N9−C4	202	anti	262	anti

Table 2. ^2J and ^3J Hetero- and Homonuclear Coupling Constants Associated with the Ribose Pucker and Backbone Torsion Angles in RNA

angle	^3J coupling constants		^2J coupling constants		
β	^3J(H5′$^{(pro-S)}$,P)	^3J(H5′$^{(pro-R)}$,P)	^3J(C4′,P)	^2J(C5′,P)	
γ	^3J(H5′$^{(pro-S)}$,H4′)	^3J(H5′$^{(pro-R)}$,H4′)	^3J(C3′,H5′$^{(pro-S)}$) ^3J(C3′,H5′$^{(pro-R)}$)	^2J(C5′,H4′)	^2J(C4′,H5′$^{(pro-S)}$) ^2J(C4′,H5′$^{(pro-R)}$)
ϵ	^3J(H3′,P)	^3J(C4′,P)	^3J(C2′,P)	^2J(C3′,P)	
ν_1	^3J(H1′,H2′)	^3J(H1′,C3′)	^3J(C3′,H1′)	^2J(C2′,H1′)	^2J(C1′,H2′)
ν_2	^3J(H2′,H3′)	^3J(C1′,H3′)	^3J(C4′,H2′)	^2J(C3′,H2′)	^2J(C2′,H3′)
ν_3, δ	^3J(H3′,H4′)	^3J(C5′,H3′)	^3J(C2′,H4′)	^2J(C3′,H4′)	^2J(C4′,H3′)
χ (pyrimidine)	^3J(H1′,C6)	^3J(H1′,C2)	^3J(H6,C1′)	^2J(H1′,N1)	^2J(H6,N1)
χ (purine)	^3J(H1′,C8)	^3J(H1′,C4)	^3J(H8,C1′)	^2J(H1′,N9)	^2J(H8,N9)

be used to determine the sugar pucker due to their pseudo-Karplus dependence on ν_1, ν_2, and ν_3.[4,6] In addition, certain ^1J(C,H) coupling constants[7,8] can be related to the sugar pucker.

The glycosidic torsion angles, χ (O4′−C1′−N1−C2) in pyrimidines (cytidine/uridine) and χ (O4′−C1′−N9−C4) in purines (guanosine/adenosine), are defined by two ^3J(C,H) couplings (Table 2). The ^3J(H1′,C) couplings to the C8,C4 carbons in purines and to the C2,C6 carbons in pyrimidines all depend on χ, although all are relatively small (1−5 Hz) in magnitude. In pyrimidines, the ^3J(H1′,C2) coupling is found to be ∼2 Hz smaller than the ^3J(H1′,C6) coupling for the anti configuration, while the opposite is true for the syn case. In purines, the ^3J(H1′,C4) coupling is found to be ∼2 Hz smaller than ^3J(H1′,C8) coupling for the anti configuration, and again the opposite is true for the syn case.[9,10] The torsion angle γ (O5′−C5′−C4′−C3′) can be determined from ^3J(H4′,H5′$^{(pro-S)}$), ^3J(H4′,H5′$^{(pro-R)}$), ^2J(C5′,H4′), ^2J(C4′,H5′$^{(pro-S)}$), and ^2J(C4′,H5′$^{(pro-R)}$) coupling constants (Table 2). The combined analysis of these couplings can also provide stereospecific assignment of geminal H5′ protons. Each of the three staggered rotamers associated with the torsion angle γ has a unique ^3J(H,H) and ^2J(C,H) coupling constant signature (Figure 3). For the gauche$^+$ rotamer both the ^3J(H4′,H5′$^{(pro-S)}$) and ^3J(H4′,H5′$^{(pro-R)}$) couplings are relatively small (<3 Hz). In contrast, for the gauche$^-$ rotamer a relatively large ^3J(H4′,H5′$^{(pro-S)}$) coupling is expected, while for the trans

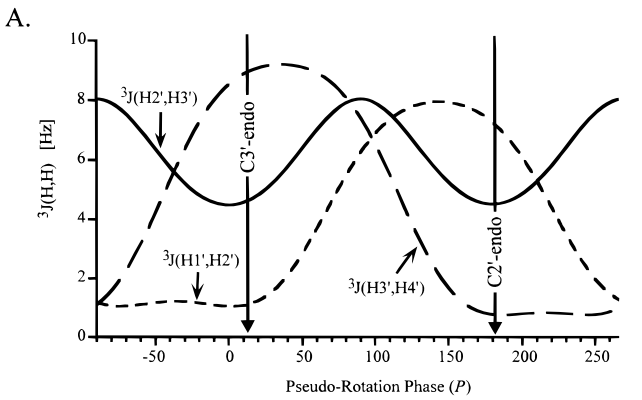

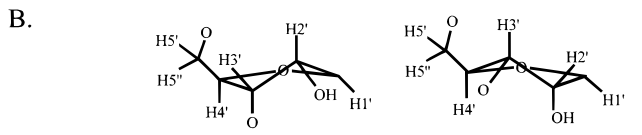

	C2'-endo (South)	C3'-endo (North)
^{3}J(H1',H2')	7.6 Hz	1.3 Hz
^{3}J(H2',H3')	4.4 Hz	3.8 Hz
^{3}J(H3',H4')	1.2 Hz	8.8 Hz
^{2}J(C1',H2')	Negative	Positive
^{2}J(C2',H3')	Negative	Positive
^{2}J(C3',H2')	Positive	Negative
^{2}J(C4',H3')	Positive	Negative

FIGURE 2. (A) Karplus curves relating ^3J(H1′,H2′), ^3J(H2′,H3′), and ^3J(H3′,H4′) couplings to the pseudorotation phase angle, *P*. (B) Schematic of the two energetically preferred ribose conformations (C2′-endo and C3′-endo) and the ^3J(H,H) and ^2J(C,H) coupling constants expected for the ν_1, ν_2, and ν_3 angles in these conformations.

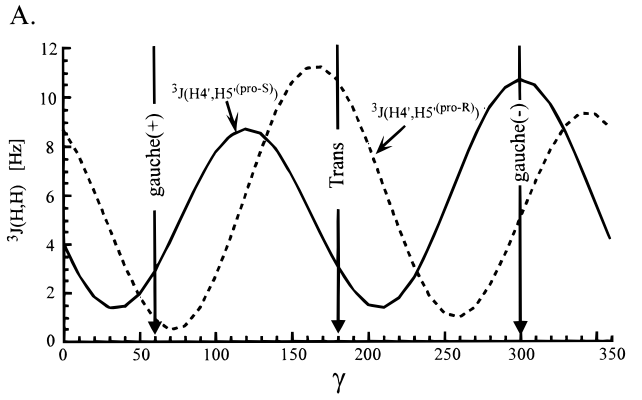

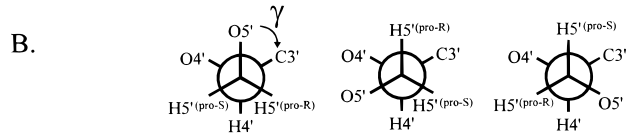

	60° (gauche$^+$)	180° (trans)	300° (gauche$^-$)
^{3}J(H4',H5'(pro-S))	~1.0 Hz	~3.0 Hz	~10.5 Hz
^{3}J(H4',H5'(pro-R))	~3.0 Hz	~10.5 Hz	~5.0 Hz
^{2}J(C4',H5'(pro-S))	negative	positive	negative
^{2}J(C4',H5'(pro-R))	positive	negative	negative
^{2}J(C5',H4')	positive	negative	negative

FIGURE 3. (A) Karplus curves relating the ^3J(H4′,H5′$^{(pro-R)}$) and ^3J(H4′,H5′$^{(pro-S)}$) couplings to corresponding torsion angles for the backbone angle γ. (B) The three energetically preferred rotamer conformations (gauche$^+$, trans, and gauche$^-$) about γ and the expected ^3J(H4′,H5′$^{(pro-R)}$), ^3J(H4′,H5′$^{(pro-S)}$), ^3J(C4′,H5′$^{(pro-R)}$), ^3J(C4′,H5′$^{(pro-S)}$), and ^3J(C5′,H4′) coupling constants for each of these conformations.

rotamer a relatively large ^3J(H4′,H5′$^{(pro-R)}$) coupling is expected. The sign and magnitude of ^2J(C4′,H5′$^{(pro-S)}$), ^2J(C4′,H5′$^{(pro-R)}$), and ^2J(C5′,H4′) couplings can also be used to assign the torsion angle about γ and stereospecifically assign the H5′ resonances.[6,11] For the gauche$^+$ rotamer, the ^2J(C4′,H5′$^{(pro-S)}$) coupling is expected to be negative and the ^2J(C4′,H5′$^{(pro-R)}$) and ^2J(C5′,H4′) couplings are expected to be positive, for the trans conformer, the ^2J(C4′,H5′$^{(pro-S)}$) coupling is expected to be positive and the ^2J(C4′,H5′$^{(pro-R)}$) and ^2J(C5′,H4′) couplings are expected to be negative, and for the gauche$^-$ conformer, all ^2J(C,H) couplings are expected to be negative. ^3J(C3′,H5′$^{(pro-S)}$) and ^3J(C3′,H5′$^{(pro-R)}$) couplings can also be used to determine the conformation about the γ angle; however, these couplings are quite difficult to measure.[4,6]

The torsion angle β (P_n−O5′−C5′−C4′) can be determined by measurement of ^3J(H5′$^{(pro-S)}$,P), ^3J(H5′$^{(pro-R)}$,P), and ^3J(C4′,P) couplings (Table 2). For the torsion angle β, the three classic staggered rotamers each have unique ^3J(H,P) and ^3J(C,P) coupling constant signatures (Figure 4). In the trans conformation, both the ^3J(P,H5′$^{(pro-R)}$) and ^3J(P,H5′$^{(pro-S)}$) couplings are small and the ^3J(P,C4′) coupling is large. If β is not trans, either the ^3J(H5′$^{(pro-S)}$,P) or ^3J(H5′$^{(pro-R)}$,P) coupling is large and stereospecific assignment of the H5′ proton resonances is necessary to distinguish between the two gauche conformers. In both the gauche rotamers, the ^3J(P,C4′) coupling is expected to be small and therefore cannot be used to distinguish between these conformations. For the torsion angle ϵ (C4′−C3′−O3′−P_{n+1}), only two of the three classic staggered rotamers are normally populated, gauche$^-$ and trans, due to steric restrictions. For both the trans and gauche$^-$ conformers, the ^3J(H3′,P) heteronuclear coupling is similar (~5 Hz). The two ^3J(C,P) coupling constants ^3J(C2′,P) and ^3J(C4′,P), however, can be used to distinguish the two conformers. The ^3J(C4′,P) coupling constant is expected to be large for ϵ in the trans conformation and small for ϵ in the gauche$^-$ conformation, while the opposite behavior is expected for the ^3J(C2′,P) coupling (Figure 5).

For the dihedral angles α ($O3'_{n+1}$−P_n−O5′−C5′) and ζ (C3′−O3′−P_{n+1}−$O5'_{n+1}$), information about the dihedral geometry cannot in practice be obtained from *J*-couplings. Frustratingly, these dihedral angles are also poorly defined by nuclear Overhauser enhancement (NOE) distance measurements. In previous NMR studies and quantum mechanical calculations, the ^{31}P chemical shift has been correlated with the conformation about α and ζ.[12,13] However, since chemical shifts can be affected by more than bond geometry, the use of ^{31}P shifts in defining α and ζ requires great caution.

^3J(H,H) Coupling Constants

The measurement of ^3J(H,H) coupling constants in RNA using ^{1}H NMR methods was limited in the past due to

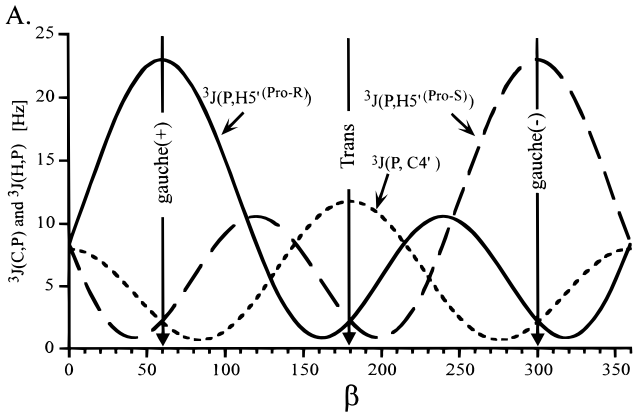

	60° (gauche$^+$)	180° (trans)	300° (gauche$^-$)
^{3}J(P,H5'(pro-S))	~2.5 Hz	~2.5 Hz	~22.5 Hz
^{3}J(P,H5'(pro-R))	~22.5 Hz	~2.5 Hz	~2.5 Hz
^{3}J(P, C4')	~2.5 Hz	~11.0 Hz	~2.5 Hz

FIGURE 4. (A) Karplus curves relating the ^3J(H5′$^{(pro-R)}$,P), ^3J(H5′$^{(pro-S)}$,P), and ^3J(C4′,P) coupling constants to corresponding torsion angles for the backbone angle β. (B) The three energetically preferred rotamer conformations (gauche$^+$, trans, and gauche$^-$) about β and the expected ^3J(H,P) and ^3J(C,P) coupling constants for each of these conformations.

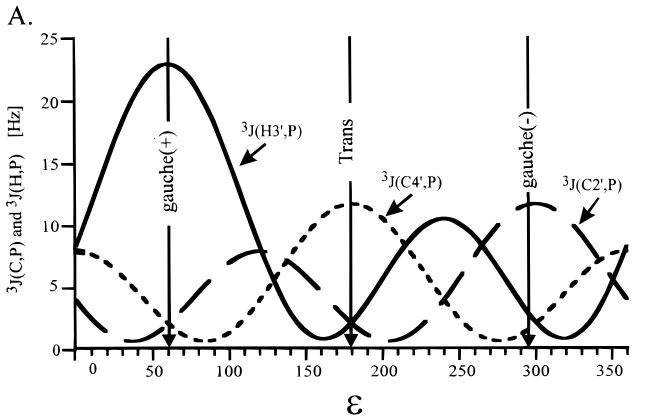

	60° (gauche$^+$)	180° (trans)	300° (gauche$^-$)
^{3}J(P,H3')	23.0 Hz	2.2 Hz	2.2 Hz
^{3}J(P,C2')	2.1 Hz	2.1 Hz	11.8 Hz
^{3}J(P, C4')	2.2 Hz	11.8 Hz	2.1 Hz

FIGURE 5. (A) Karplus curves relating the ^3J(H3′,P) and ^3J(C2′,P) couplings to the corresponding torsion angles for the backbone angle ϵ. (B) The three energetically preferred rotamer conformations (gauche$^+$, trans, and gauche$^-$) about ϵ and the expected ^3J(H3′,P) and ^3J(C2′,P) coupling constants for each of these conformations.

both difficulties in resolving ribose proton resonance and broad proton line widths. Initial attempts to determine ^3J(H,H) couplings were made by analysis of the in-phase passive and anti-phase splittings observed in double-quantum filtered correlation spectroscopy (DQF-COSY)[14] and primitive exclusive correlation spectroscopy (P.E.COSY)[15] spectra. The ^3J(H,H) couplings were estimated from the separations observed in the multiplets of the correlated cross-peaks with weak or absent peaks indicative of small couplings on the order of the line width.

Recently, access to uniformly ^{13}C,^{15}N labeled RNA oligonucleotides[16−18] has allowed the development of multidimensional double and triple resonance NMR experiments for determining *J*-couplings. With uniform ^{13}C labeling of the ribose sugar, ^3J(H1′,H2′), ^3J(H2′,H3′), and ^3J(H3′,H4′) couplings, which define the ribose conformation, and ^3J(H4′, H5′$^{(pro-R)}$) and ^3J(H4′, H5′$^{(pro-S)}$) couplings, which define the angle γ, can now be measured using a proton−carbon−carbon−proton exclusive correlation spectroscopy (HCCH-E.COSY) experiment.[19,20] The HCCH-E.COSY experiment allows the measurement of both the magnitude and the sign of these ^3J(H[*i*]′,H-[*i*+1]′) couplings. In the experiment, three mutually coupled spins, H[*i*]′, C[*i*]′ and H[*i*+1]′, which can be represented by an "E.COSY triangle" (Figure 6A), are used to generate a cross-peak that is located at the chemical shift of C[*i*]′ and split by the relatively large ^1J(H[*i*]′,C[*i*]′) coupling (~160 Hz) in one dimension and located at the chemical shift of H[*i*+1]′ and split by the small ^3J(H[*i*]′,H-[*i*+1]′) coupling in the second dimension (Figure 6A). The resulting cross-peak structure resolves the small ^3J(H[*i*]′,H-[*i*+1]′) couplings so that these couplings can be accurately measured. The HCCH-E.COSY can be measured as either a two- or three-dimensional (2D or 3D) experiment, where the third dimension is chosen on the basis of the relative resolving power of the correlated ^{1}H and ^{13}C resonances. The HCCH-E.COSY has been shown to have sufficient resolution and sensitivity to measure a rather complete set of ^3J(H1′,H2′) couplings in moderately sized RNAs (Figure 6B).[20]

In practice, the HCCH-E.COSY experiment does not provide sufficient resolution to measure most ^3J(H[*i*]′,H-[*i*+1]′) couplings since they are derived from (C2′,H3′), (C3′,H2′), (C3′,H4′), (C4′,H3′), and (C4′,H5′) cross-peaks, which are overlapped either mutually or with (C2′,H2′), (C3′,H3′), and (C4′,H4′) cross-peaks. To increase resolution, these *J*-couplings can be measured using a "directed" HCC-TOCSY−CCH-E.COSY experiment.[11,21,22] The directed HCC-TOCSY−CCH-E.COSY experiment, which is an obligatory 3D experiment, achieves higher resolution and sensitivity by employing an extremely selective magnetization transfer step between the H1′ proton and the C[*i*],H[*i*+1] HCCH−COSY cross-peaks within the ribose ring.[22] As a result, the experiment yields only the (C1′,-H2′), (C2′,H3′), (C3′,H4′), and (C4′,H5′) HCCH−COSY cross-peaks that are resolved in the third dimension by the H1′ proton chemical shift (Figure 7).

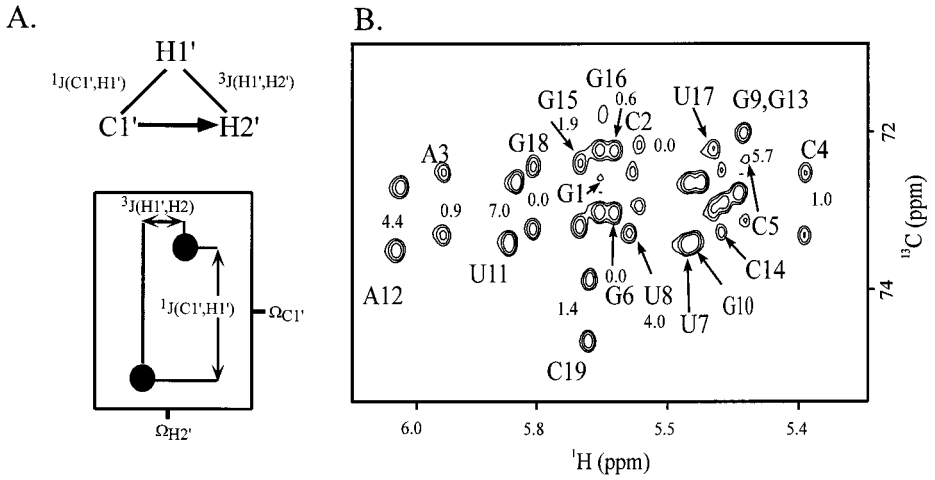

FIGURE 6. A schematic triangle (A) which "connects" the three-spin system that is correlated in the HCCH-E.COSY experiment and a schematic of the expected cross-peak multiplet pattern. (B) The C2′,H1′ region of the 2D HCCH-E.COSY experiment of a uniformly ^{13}C,^{15}N labeled 19-mer RNA hairpin with the ^3J(H1′,H2′) coupling constants and resonance assignments indicated.

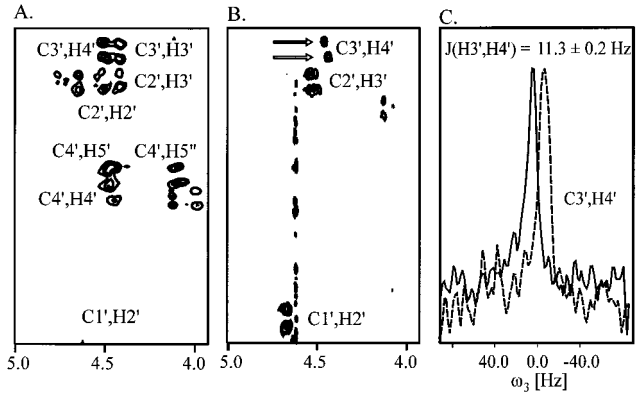

FIGURE 7. Slices taken in the H1′ dimension of nondirected (A) and directed (B) 3D HCC-TOCSY−CCH-E.COSY experiments on a uniformly ^{13}C,^{15}N labeled 19-mer RNA hairpin. The directed HCC-TOCSY−CCH-E.COSY experiment is implemented with constant time and TOCSY mixing delays that are optimized for maximal transfer of the C1′ magnetization to C2′ and C3′ carbons. Panel C shows traces through the C3′,H4′ cross-peak together with couplings derived using a fitting procedure described in ref 20.

^nJ(H,C) Coupling Constants

^3J(H,C) and ^2J(H,C) coupling constants have been measured in RNA using E.COSY[23,24] methods. Using a 30% randomly ^{13}C labeled RNA oligonucleotide, ^3J(H,C) and ^2J(H,C) couplings have been measured using X-filtered nuclear Overhauser spectroscopy (NOESY) and total correlation spectroscopy (TOCSY) experiments where ^{13}C-decoupling was left out in either ^1H dimension to generate the desired E.COSY multiplet pattern.[4,6] The dilute isotopic labeling of 30% was used to simplify the cross-peak pattern and to reduce the influence of passive $^{13}C-^{13}C$ splittings. Although successful in measuring a number of couplings, these X-filtered experiments suffer significantly from insensitivity and cross-peak overlap. More recently, a set of experiments based on CH-selective HSQC correlation have been used to measure a more complete set of ^2J(C4′,H5′) couplings.[11] As in the HCCH-E.COSY, three mutually coupled spins, H[i]′, C[i]′, and C[i+1]′, which can be represented by an E.COSY triangle (Figure 8A), are used

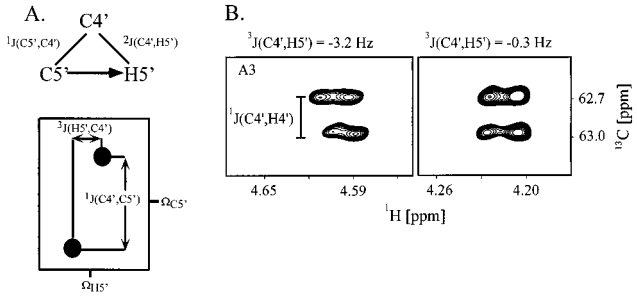

FIGURE 8. (A) A schematic triangle which "connects" the three-spin system that is correlated in the selective CT-HSQC E.COSY experiment and a schematic of the expected cross-peak multiplet pattern. (B) A C5′H5′ cross-peak from a 2D HSQC experiment performed on the uniformly ^{13}C,^{15}N labeled 19-mer RNA hairpin with ^3J(C4′,H5′) couplings and resonance assignments indicated.

to generate a cross-peak that is located at the chemical shift of C[i]′ and split by the relatively large ^1J(C[i]′,C[i+1]′) coupling (~40 Hz) in one dimension and located at the chemical shift of H[i]′ and split by the small ^2J(H[i]′,C-[i+1]′) coupling in the second dimension (Figure 8A). The resulting cross-peak structure which is generated again allows the resolution and accurate measurement of the small ^2J(H[i]′,C[i+1]′) couplings (Figure 8B). A 3D version of the CH-selective HSQC pulse sequence can be implemented using the evolution of an additional resonance that is correlated by an additional transfer step.

^3J(H,C) coupling constants have also been measured in RNA using the quantitative-J[25] method. In a quantitative-J type experiment, J-couplings are extracted from a quantitative evaluation of cross-peak intensities generated by the active J-coupling. For example, the size of ^3J(H,C) couplings, associated with the torsion angle χ about the glycosidic bond, has been determined using the relative intensities of cross-peaks generated in a refocused heteronuclear multiple bond correlation (HMBC) experiment. If the dependence of the relative transfer amplitude on the active coupling constant is known in experiment, then the size of the interesting coupling can be deduced by comparing its cross-peak intensity with the intensity of a

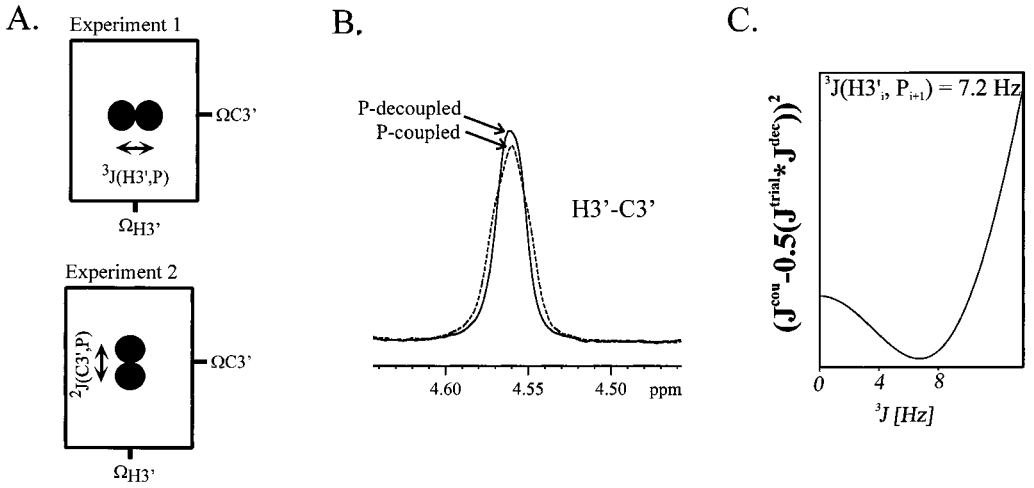

FIGURE 9. (A) Schematic of the multiplet pattern expected in the two P-FIDS−CT-HSQC experiments. (B) Traces of the C3′,H3′ cross-peak in the P-FIDS−CT-HSQC experiment displaying the differences due to *J*(H,P) coupling evolution (the solid line is ^{31}P decoupled, and the dashed line is ^{31}P coupled). Representative traces taken from the uridine residue in a 10-mer RNA with uniformly ^{13}C labeled in the uridine ribose moieties. (C) Fitting of the two rows extracted from the experiment according to ref 20.

cross-peak with a known coupling. ^3J(H1′,C8) and ^3J(H1′,C4) couplings in purines and ^3J(H1′,C6) and ^3J(H1′,C2) couplings in pyrimidines have been determined using this method by comparison of the cross-peak intensity of the long-range C,H1′ correlation with the intensity of the C1′,H1′ cross-peak.[10,20,26]

^3J(H,P) and ^3J(C,P) Coupling Constants

The vicinal ^nJ(H,P) coupling constants can be measured in principle from the line splitting found in the correlated cross-peaks of an ^{1}H,^{31}P heteronuclear COSY experiment (or so-called HETCOR experiment).[27] However, cross-peak overlap and complications due to additional homonuclear couplings make interpretation of HETCOR cross-peak multiplets difficult. More recently, ^nJ(H,P) and ^nJ(C,P) heteronuclear couplings have been measured in uniformly ^{13}C labeled RNA using both phosphorus-fitting of doublets from singlets (P-FIDS)[20,28] and spin−echo difference[29] methods. In the P-FIDS method, the magnitude of the *J*-coupling is calculated by comparison of peak multiplet patterns in spectra collected with and without ^{31}P-decoupling during either a constant time (CT) carbon chemical shift evolution period or a proton chemical shift acquisition period. Since spectra can be collected with ^{31}P-decoupling of either the carbon or proton chemical shift evolution periods, the P-FIDS method allows both ^nJ(H,P) and ^nJ(C,P) couplings to be measured. ^nJ(H,P) and ^nJ(C,P) couplings are determined using a routine that fits ^{31}P-coupled cross-peaks to simulated cross-peaks generated from a reference experiment, where ^{31}P-decoupling is employed, and a trial *J*-coupling (Figure 9).

The spin−echo CT-HSQC experiment[29] is a second method that has been applied to quantitatively measure ^3J(C,P) coupling constants in RNA.[30,31] In these spectra the magnitude of the *J*-coupling is calculated by comparison of cross-peak intensity in spectra collected with and without ^{31}P-decoupling during the CT carbon chemical shift evolution. In the ^{31}P-coupled spectra, the cross-peak intensity (I) is modulated according to $\cos(\pi J_{CP}\tau)$, where J_{CP} is the desired coupling and τ a CT evolution period. In the ^{31}P-decoupled reference spectra, the cross-peak intensity (I) is independent of the J_{CP} coupling.

One problem inherent in both of these methods is the inability to obtain individual estimates for the $^3J(C4'_i,P_i)$ and $^3J(C4'_i,P_{i+1})$ couplings because each C4′ nucleus is coupled to two ^{31}P nuclei at the same time. Since only the intensity or sum of the line-broadening can be measured, only sums of couplings rather than individual values can be obtained for the sequential $^3J(C4'_{i-1},P)$ and the intraresidual ^3J(P,C4′) coupling constants. These couplings can be deconvoluted from each other using a recently developed quantitative-*J* HCP experiment (Figure 10).[32] In the quantitative-*J* HCP experiment,[33,34] the differential coupling dependence of the H4′ → C4′ → P_i and H4′ → C4′ → P_{i+1} correlations can be used to determine unique ^3J(C4′,P) couplings by comparison to a reference experiment where both ^3J(C4′,P) couplings attenuate the intensity of the H4′,C4′ cross-peak.

J-Coupling Constants and Dihedral Angle Restraints

Torsion angles, which are consistent with the measured *J*-couplings, can be determined using theoretical Karplus relationships that have been empirically parametrized. Karplus relationships have been parametrized for H−C−C−H, C−C−C−H, C−C−O−P, and H−C−O−P fragments in nucleic acids.[35−37] For ^3J-couplings between two protons in the ribose ring the best-fit Karplus relation (Figures 2 and 3) is[35,38]

$$^3J(H,H) = 13.7\cos^2\phi - 0.73\cos\phi + \sum_i \Delta\chi_i\{0.56 - 2.47\cos^2(z_i\phi + 16.9|\Delta\chi_i|)\} \quad (1)$$

where ϕ is the torsion angle and $\Delta\chi$ and z_i depend on the electronic character and orientation, respectively, of non-proton substituents on the carbon atoms with $\Delta\chi$ = O,

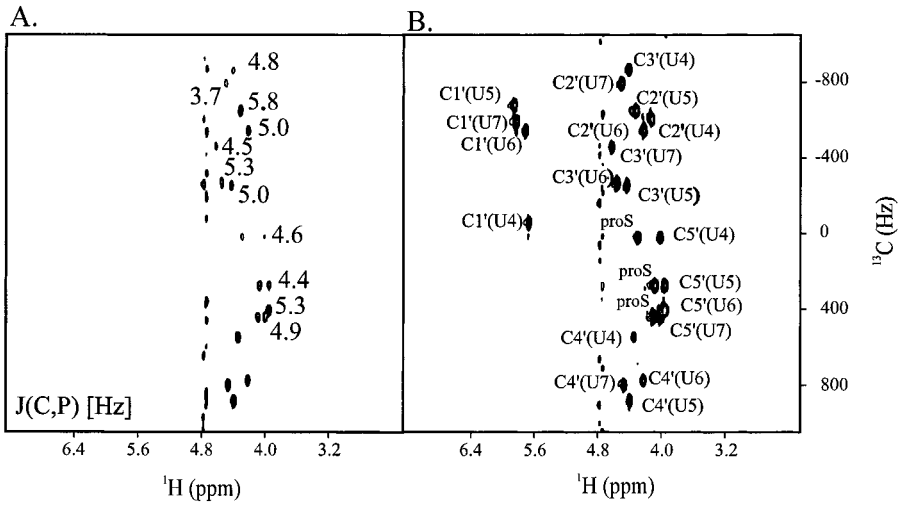

FIGURE 10. 2D cross-peak selected (A) and reference (B) HC(P) experiment applied to a 10-mer RNA uniformly ^{13}C labeled in the uridine ribose moieties. ^{2}J(C3′,P), ^{2}J(C5′,P), and ^{3}J(C2′,P) coupling constants together with resonance assignments and stereospecific assignments are shown.

1.3; C, 0.4; N, 0.85; and P, −0.05 and $z_i = \pm 1$. For ^{3}J-couplings between proton and carbon (C−C−C−H) fragments the best-fit Karplus relation is[5,39,40]

$$^{3}J(\mathrm{C,H}) = 5.7\cos^2\phi - 0.6\cos\phi + 0.5 \qquad (2)$$

For ^{3}J-couplings between proton and phosphorus and carbon and phosphorus[37,41,42] the best-fit Karplus relations (Figures 4 and 5) are

$$^{3}J(\mathrm{H,P}) = 15.3\cos^2\phi - 6.1\cos\phi + 1.6 \qquad (3)$$

$$^{3}J(\mathrm{C,P}) = 6.9\cos^2\phi - 3.4\cos\phi + 0.7 \qquad (4)$$

Despite the availability of parametrized Karplus relations for interpretation of ^{3}J-couplings in nucleic acids, the level of precision to which these relations have been parametrized for heteronuclear ^{3}J-couplings is quite low. Additional studies of model compounds, together with an increase in the database of measured J-couplings in RNA, will therefore be required to improve the precision to which J-couplings can be fit.

Dihedral Angle Restraints in RNA Structure Determination

NOE-derived distance restraints are the primary source of structural information used in protein structure determination by NMR spectroscopy.[43,44] Using multidimensional ^{15}N and ^{13}C edited/selected NOESY experiments, large NOE data sets are now routinely collected for ^{13}C,^{15}N-labeled proteins and complexes of ^{13}C,^{15}N-labeled proteins with nucleic acids, peptides, and other ligands. These same NOESY experiments can be applied to ^{13}C,^{15}N-labeled RNA oligonucleotides.[45] In contrast to proteins, however, NOE data alone are normally not sufficient for the determination of high-resolution structures of RNA. This is because the proton density and thus the number of NOE-derived distance restraints are lower in RNA relative to proteins, while the number of backbone degrees of freedom is higher. In addition, the dihedral angles that define the phosphodiester backbone and sugar conformations are essentially undefined by NOE data. J-coupling constants, which can be related directly to phosphodiester backbone and sugar dihedral angles using parametrized Karplus relations, therefore provide more significant restraints in the structure determination of RNA oligonucleotides when compared with proteins.[46] Recent NMR structural studies[45,47−49] of RNA and RNA−protein complexes have to a large extent incorporated torsion angle restraints, together with distance restraints based on semiquantified NOEs, into distance geometry and restrained simulated annealing protocols to produce high-resolution structures. Like NOEs, the torsion angle restraints have been implemented in most cases in a semiquantitative fashion, usually restricting an angle to one of the three possible staggered rotamer conformations. Nonetheless, even at this rather crude level of implementation of the measured torsion angles, an effect on both the precision and accuracy of the structures has been observed.[50,51] The most dramatic effect of using dihedral restraints in the NMR-derived structure calculations is improvement in the accuracy of the determined structures. With a large number of NOE-derived distance restraints, rather precise structures can now be determined. Nonetheless, in these families of structures, convergence to the correct local dihedral geometry is generally poor. When dihedral restraints have been applied in a semiquantitative way to the refinement steps of these structure calculations, however, the local dihedral geometry converges to both the precise and more accurate configuration.

In areas of RNA molecules where the NOE density is particularly sparse, the dihedral restraints have had a larger impact on the precision of the structure. In these poorly determined regions of the RNA structure, the additional restraints have the expected effect of increasing both the precision and accuracy of the backbone geometry (Figure 11). Still, however, the structural homogeneity is usually still far less pronounced in these structural regions.

Table 3. A Summary of NMR Methods Used To Determine ^2J and ^3J Hetero- and Homonuclear Coupling Constants

experiment	measured coupling constants
HCCH-E.COSY	^3J(H1′,H2′)
directed HCC-TOCSY−CCH-E.COSY	^3J(H1′,H2′), ^3J(H2′,H3′), ^3J(H3′,H4′), ^3J(H5′$^{(pro-S)}$,H4′), ^3J(H5′$^{(pro-R)}$,H4′)
CH-selective CT-HSQC	^2J(C4′,H5′$^{(pro-S)}$), ^2J(C4′,H5′$^{(pro-R)}$), ^2J(C2′,H1′)
quantitative HMBC	^3J(H1′,C2), ^3J(H1′,C4), ^3J(H1′,C8), ^3J(H1′,C6)
P-FIDS−CT-HSQC	^3J(H5′$^{(pro-S)}$,P), ^3J(H5′$^{(pro-R)}$,P), ^3J(H3′,P), ^2J(C5′,P), ^2J(C3′,P), ^3J(C2′,P)
spin−echo difference CT-HSQC	^2J(C5′,P), ^2J(C3′,P), ^3J(C2′,P)
quantitative HCP	^3J(C4′,P), ^2J(C5′,P), ^2J(C3′,P), ^3J(C2′,P)

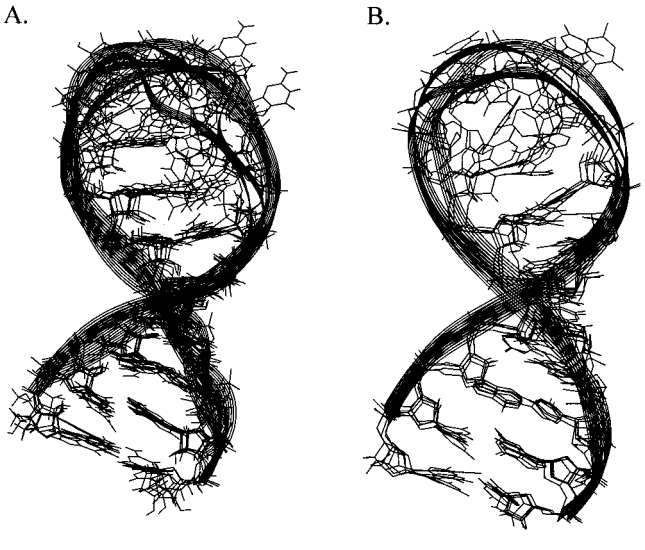

FIGURE 11. Two overlays showing the 19-mer 5′-GCACCGUUG-GUAGCGGUGC-3′ stem−loop from the four lowest energy structures generated using (A) a full list of NOE restraints including NOEs stereospecifically assigned to the H5′ protons and (B) all NOEs together with dihedral restraints. The pairwise rmsd calculated for all heavy atoms in the loop region of the structure decreased from 3.6−5.0 Å for the group of structures (A) calculated with only NOE restraints to 1.3−1.9 Å for the group of structures (B) calculated with NOE and dihedral restraints.

Whether this is a faithful description of the structure in solution or simply reflects a deficiency of data is not yet well-known.

Conclusion and Future Prospects

A number of sensitive heteronuclear NMR methods have been developed in recent years to determine *J*-couplings for RNAs up to 30 nucleotides in size (Table 3). These methods have allowed access to a more complete set of *J*-couplings for RNA molecules in this size range and thereby have provided additional torsion angle restraints. To apply these methods to even larger RNAs where chemical shift overlap becomes chronic, methods available for specific isotope labeling will have to be used.

In the future, a more rigorous treatment of averaged *J*-couplings in structure calculations will also be required to better represent conformational heterogeneity. Currently, torsion angle restraints are applied primarily in a static fashion in RNA structure determination. One possibility will be to incorporate average *J*-couplings as time-averaged restraints.[52,53] NMR methods are also being developed to measure cross-correlated relaxation rates[54] between C,H bond vectors and the ^{31}P chemical shift anisotropy (CSA) tensor. Such measurements may provide for the first time a direct measure of the backbone angles α and ζ. Last, exciting new NMR methods designed to measure residual dipolar couplings in very slightly oriented macromolecules are also currently being developed.[55−57] These methods show great promise for providing the first NMR-derived information about long-range structure and dynamics in RNA.

We acknowledge support from the Fonds der Chemischen Industrie and the DFG. J.P.M. acknowledges a Humboldt postdoctoral fellowship. H.S. acknowledges a fellowship from the European Large Scale NMR Facility. We thank our co-workers (Donald Crothers, Steffen Glaser, Thorsten Naumann, Bernd Reif, and Christian Richter) who have all contributed to our work with RNA.

References

(1) Karplus, M. *J. Chem. Phys.* **1959**, *30*, 11.
(2) Altona, C. Conformation Analysis of Nucleic Acids. Determination of Backbone Geometry of Single-helical RNA and DNA in Aqueous Solution. *Recl. Trav. Chim. Pays-Bas* **1982**, *101*, 413−433.
(3) Saenger, W. *Principles of Nucleic Acid Structure*; Springer-Verlag: New York, 1988.
(4) Hines, J. V.; Landry, S. M.; Varani, G.; Tinoco, I., Jr. Carbon-Proton Scalar Couplings in RNA: 3D Heteronuclear and 2D Isotope-edited NMR of a ^{13}C-Labeled Extra-Stable Hairpin. *J. Am. Chem. Soc.* **1994**, *116*, 5823−5831.
(5) Kline, P. C.; Serianni, A. S. ^{13}C-Enriched Ribonucleosides: Synthesis and Application of ^{13}C-^{1}H and ^{13}C-^{13}C Spin-Coupling Constants to Assess Furanose and N-glycoside Bond Conformations. *J. Am. Chem. Soc.* **1990**, *112*, 7373−81.
(6) Hines, J. V.; Varani, G.; Landry, S. M.; Tinoco, I. J. The stereospecific assignment of H5′ and H5″ in RNA using the sign of two-bond carbon-proton scalar couplings. *J. Am. Chem. Soc.* **1993**, *115*, 11002−3.
(7) Varani, G.; Tinoco, I., Jr. Carbon Assignments and Heteronuclear Coupling Constants for an RNA Oligonucleotide from Natural Abundance 13C-1H Correlated Experiments. *J. Am. Chem. Soc.* **1991**, *113*, 9349−9354.
(8) Serianni, A. S.; Wu, J.; Carmicheal, I. One-Bond ^{13}C-^{1}H Spin-Coupling Constants in Aldopyranoside Rings − Effect of Conformation on Coupling Magnitude. *J. Am. Chem. Soc.* **1995**, *117*, 8645−8650.
(9) Davies, D. B.; Rajani, P.; MacCoss, M.; Danyluk, S. S. Determination of the Karplus Relationships for the C-2, H-1′ and C-6, H-1′ Vicinal Coupling Paths of Uridine Derivatives. *Magn. Reson. Chem.* **1985**, *23*, 72−77.

(10) Zimmer, D.; Marino, J.; Griesinger, C. Determination of Homo- and Heteronuclear Coupling Constants in Uniformly ^{13}C,^{15}N Labeled DNA Oligonucleotides. *Magn. Reson. Chem.* **1997**, *34*, 177−186.
(11) Marino, J. P.; Schwalbe, H.; Glaser, S. J.; Griesinger, C. Determination of γ and Stereospecific Assignment of ^{2}J and ^{3}J coupling Constants in Uniformly ^{13}C labeled RNA, *J. Am. Chem. Soc.* **1996**, *118*, 4388−4395.
(12) Gorenstein, D. G. ^{31}P NMR of DNA. *Methods Enzymol.* **1992**, *211*, 254−86.
(13) Giessner-Prettre, C.; Pullman, B. Quantum Mechanical Calculations of NMR Chemical Shifts in Nucleic Acids. *Q. Rev. Biophys.* **1987**, *20*, 113−172.
(14) Varani, G.; Cheong, C.; Tinoco, I. J. Structure of an unusually stable RNA hairpin. *Biochemistry* **1991**, *30*, 3280−9.
(15) Müller, L. P. E. COSY, A Simple Alternative to E. COSY. *J. Magn. Reson.* **1987**, *72*, 191−196.
(16) Batey, R. T.; Inada, M.; Kujawinski, E.; Puglisi, J. D.; Williamson, J. R. Preparation of isotopically labeled ribonucleotides for multidimensional NMR spectroscopy of RNA. *Nucleic Acids Res.* **1992**, *20*, 4515−23.
(17) Nikonowicz, E. P.; Sirr, A.; Legault, P.; Jucker, F. M.; Baer, L. M.; Pardi, A. Preparation of ^{13}C and ^{15}N labelled RNAs for Heteronuclear Multi-dimensional NMR Studies. *Nucleic Acids Res.* **1992**, *20*, 4507−13.
(18) Quant, S.; Wechselberger, R. W.; Wolter, M. A.; Worner, K. H.; Schell, P.; Engels, J. W.; Griesinger, C.; Schwalbe, H. Chemical Synthesis ^{13}C Labeled RNA and DNA monomers for the Solid Phase and Template Controlled Enymatic synthesis of DNA and RNA Oligomers. *Tetrahedron Lett.* **1994**, *35*, 6649−52.
(19) Griesinger, C.; Eggenberger, U. Determination of Proton−Proton Coupling Constants in ^{13}C-Labeled Molecules. *J. Magn. Reson.* **1992**, *75*, 426−434.
(20) Schwalbe, H.; Marino, J. P.; King, G. C.; Wechselberger, R.; Bermel, W.; Griesinger, C. Determination of a complete set of coupling constants in ^{13}C-labeled oligonucleotides. *J. Biomol. NMR* **1994**, *4*, 631−44.
(21) Schwalbe, H.; Marino, J. P.; Glaser, S. J.; Griesinger, C. Measurement of H, H.-Coupling Constants Associated with v_1, v_2 and v_3 in Uniformly ^{13}C-labeled RNA by HCC-TOCSY−CCH-ECOSY. *J. Am. Chem. Soc.* **1995**, *117*, 7251−7252.
(22) Glaser, S.; Schwalbe, H.; Marino, J. P.; Griesinger, S. Directed TOCSY, a Method for Selection of Directed Correlations by Optimal Combinations of Isotropic and Longitudinal Mixing. *J. Magn. Reson.* **1996**, *B112*, 160−180.
(23) Griesinger, C.; Sørensen, O. W.; Ersnt, R. R. Two-Dimensional Correlation of Connected NMR Transitions. *J. Am. Chem. Soc.* **1985**, *107*, 6394−6396.
(24) Griesinger, C.; Sørensen, O. W.; Ernst, R. R. Practical Aspects of the E. COSY Technique. Measurement of Scalar Spin−Spin Coupling Constants in Peptides. *J. Magn. Reson.* **1987**, *75*, 474−492.
(25) Bax, A.; Vuister, G. W.; Grzesiek, S.; Delaglio, F.; Wang, A. C.; Tschudin, R.; Zhu, G. Measurement of Homonuclear and Heteronuclear J-Couplings from Quantitative J-Correlation. *Methods Enzymol.* **1994**, *239*, 79−105.
(26) Zhu, G.; Live, D.; Bax, A. Analysis of Sugar Puckers and Glycosidic Torsion Angles in a DNA G-Tetrad Structure by Heteronuclear Three-Bond J Coupling. *J. Am. Chem. Soc.* **1994**, *116*, 8370−8371.
(27) Sklenar, V.; Miyashiro, H.; Zon, G.; Miles, H. T.; A., B. Assignment of the ^{31}P and ^{1}H Resonances in Oligonucleotides by Two-dimensional NMR Spectroscopy. *FEBS* **1986**, *208*, 94−98.
(28) Schwalbe, H.; Samstag, W.; Engels, J. W.; Bermel, W.; Griesinger, C. Determination of $^{3}J(C,P)$ and $^{3}J(H,P)$ Coupling Constants in Nucleotide Oligomers with FIDS−HSQC. *J. Biomol. NMR* **1993**, *3*, 479−486.
(29) Vuister, G. W.; Wang, A. C.; Bax, A. Measurement of Three-Bond Nitrogen−Carbon J Couplings in Proteins Uniformly Enriched in ^{15}N and ^{13}C. *J. Am. Chem. Soc.* **1993**, *115*, 5334−5335.
(30) Legault, P.; Jucker, F. M.; Pardi, A. Improved Measurement of ^{13}C, ^{31}P J coupling constants in Isotopically Labeled RNA. *FEBS Lett.* **1995**, *362*, 156−60.
(31) Hoogstraten, C.; Pardi, A. Measuring of Carbon-Phosphorus J Coupling Constants in RNA using Spin-Echo Difference Constant Time HCCH-COSY. *J. Magn. Reson.* **1998**, *133*, 236−240.
(32) Richter, C.; Reif, B.; Worner, K.; Quant, S.; Marino, J.; Engels, J.; Griesinger, C.; Schwalbe, H. A New Experiment for the Measurement of $^{3}J(C, P)$ Coupling Constants including $^{3}J(C4'i,Pi)$ and $^{3}J(C4'i,-Pi+1)$ in Oligonucleotides. *J. Biomol. NMR* **1998**, *12*, 223−230.
(33) Heus, H. A.; Wijmenga, S. S.; van deVen, F. J. M.; Hilbers, C. W. Sequential Backbone Assignment in ^{13}C-Labeled RNA via Through-bond Coherence transfer Using Three-Dimensional Triple Resonance Spectroscopy (^{1}H, ^{13}C, ^{31}P) and Two-Dimensional HeteroTOCSY. *J. Am. Chem. Soc.* **1994**, *116*, 4983−4984.
(34) Marino, J. P.; Schwalbe, H.; Anklin, C.; Bermel, W.; Crothers, D. M.; Griesinger, C. Three-Dimensional Triple-Resonance ^{1}H, ^{13}C, ^{31}P Experiment: Sequential Through-Bond Correlation of Ribose Protons and Intervening Phosphorus along the RNA Oligonucleotide Backbone. *J. Am. Chem. Soc.* **1994**, *116*, 6472−3.
(35) van Wijk, J.; Huckriede, B. D.; Ippel, J. H.; Altona, C. Furanose Sugar Conformation in DNA from NMR Coupling Constants. *Methods Enzymol.* **1992**, *211*, 286−306.
(36) Lankhorst, P. P.; Haasnoot, C. A.; Erkelens, C.; Westerink, H. P.; van der Marel, G. A.; van, B., J. H.; Altona, C. Carbon-13 NMR in conformational analysis of nucleic acid fragments. 4. The torsion angle distribution about the C3′−O3′ bond in DNA constituents. *Nucleic Acids Res.* **1985**, *13*, 927−42.
(37) Plavec, J.; Chattopadhyaya, J. Reparameterization of the Karplus Equation Relating $^{3}J_{C-C-O-P}$ to Torsion Angle. *Tetrahedron Lett.* **1995**, *36*, 1949−1952.
(38) Haasnoot, C. A.; de Leeuw, F. A. A. M.; Altona, C. The relationship between proton−proton NMR coupling constants and substituent electronegativities. I, an empirical generalization of the Karplus equation. *Tetrahedron* **1980**, *36*, 2783−2792.
(39) Tvaroska, I.; Hricovini, M.; Petrakova, E. An Attempt to Derive a New Karplus-Type Equation of Vicinal Proton Carbon Coupling Constants for C-O-C-H Segments of Bonded Atoms. *Carbohydr. Res.* **1989**, *189*, 359−362.
(40) Podlasek, C.; Stripe, W.; Carmichael, I.; Shang, M.; Basu, B.; Serianni, A. ^{13}C-^{1}H Spin-coupling Constants in the β-D-Ribofuranosyl Ring: Effect of Ring Conformation on Coupling Magnitudes. *J. Am. Chem. Soc.* **1996**, *118*, 1413−1425.

(41) Lankhorst, P. P.; Haasnoot, C. A.; Erkelens, C.; Altona, C. Carbon-13 NMR in conformational analysis of nucleic acid fragments. 2. A reparametrization of the Karplus equation for vicinal NMR coupling constants in CCOP and HCOP fragments. *J. Biomol. Struct. Dyn.* **1984**, *1*, 1387−405.
(42) Mooren, M. M.; Wijmenga, S. S.; van, d. M. G.; van, B. J.; Hilbers, C. W. The solution structure of the circular trinucleotide cr(GpGpGp) determined by NMR and molecular mechanics calculation. *Nucleic Acids Res.* **1994**, *22*, 2658−66.
(43) Wüthrich, K. *NMR of Proteins and Nucleic Acids*; Wiley: New York, 1986.
(44) Cavanagh, J.; Fairbrother, W.; Palmer, A.; Skelton, N. *Protein NMR Spectroscopy: Principles and Practice*; Academic Press, Inc.: New York, 1995.
(45) Varani, G.; Aboul-ela, F.; Allain, F. H.-T. NMR Investigation of RNA Structure. *Prog. Nucl. Reson. Spectrosc.* **1996**, *29*, 51−127.
(46) Wijmenga, S. S.; Mooren, M. M. W.; Hilbers, C. W. In *NMR of Macromolecules, A Practical Approach*; Roberts, G. C. K., Ed.; Oxford University Press: 1993; p 217.
(47) Chang, K.; Varani, G. Nucleic Acids Structure and Recognition. *Nat. Struct. Biol.* **1997**, *4*, 854−858.
(48) Ramos, A.; Gubser, C.; Varani, G. Recent Solution Structures of RNA and its Complexes with Drugs, peptides and proteins. *Curr. Opin. Struct. Biol.* **1997**, *7*, 317−323.
(49) Uhlenbeck, O.; Pardi, A.; Feigon, J. RNA Structure Comes of Age. *Cell* **1997**, *90*, 833−840.
(50) Allain, F. H.-T.; Varani, G. Structure of the P1 Helix from Group I Self-splicing Introns. *J. Mol. Biol.* **1995**, *250*, 333−353.
(51) Allain, F. H.-T.; Varani, G. How Accurately and precisely can RNA structure be determined by NMR. *J. Mol. Biol.* **1997**, *267*, 338−351.
(52) Schmitz, U.; Kumar, A.; James, T. L. Dynamic Interpretation of NMR Data-Molecular-Dynamics with Weighted Time-Averaged Restraints and Ensembe R-factor. *J. Am. Chem. Soc.* **1992**, *114*, 10654−10656.
(53) Pearlman, D. A. How well do time-average J-coupling restraints work? *J. Biomol. NMR* **1994**, *4*, 279−299.
(54) Reif, B.; Hennig, M.; Griesinger, C. Direct Measure of Angles Between Bond Vectors in High-Resolution NMR. *Science* **1997**, *276*, 1230−1233.
(55) Tolman, J.; Flanagan, J.; Kennedy, M.; Prestegard, J. Nuclear Magnetic Dipole Interactions in Field-Oriented Proteins: Information for Structure Determination in Solution. *Proc. Natl. Acad. Sci. U.S.A.* **1995**, *92*, 9279−9283.
(56) Tjandra, N.; Omichinski, J.; Gronenborn, A.; Clore, G.; Bax, A. Use of Dipolar ^{1}H-^{15}N and ^{1}H-^{13}C Couplings in the Structure Determination of Magnetically Oriented Macromolecules in Solution. *Nat. Struct. Biol.* **1997**, *4*, 732−738.
(57) Tjandra, N.; Bax, A. Direct Measurement of Distance and Angles in Biomolecules by NMR in a Dilute Liquid Crystalline Medium. *Science* **1997**, *278*, 1111−1114.

AR9600392